DOI: 10.1002/ejic.200600830

Valence-State Distribution in the Ruthenium *o*-Quinonoid Systems [Ru(trpy)(Cl)(L^1)]$^+$ and [Ru(trpy)(Cl)(L^2)]$^+$ (L^1 = *o*-Iminobenzoquinone, L^2 = *o*-Diiminobenzoquinone; trpy = 2,2′:6′,2′′-Terpyridine)

Somnath Maji,[a] Srikanta Patra,[a] Saumen Chakraborty,[a] Deepa Janardanan,[a] Shaikh M. Mobin,[a] Raghavan B. Sunoj,*[a] and Goutam Kumar Lahiri*[a]

Keywords: Ruthenium / Quinonoid ligands / Valence-state distributions / Density functional calculations / Spectroelectrochemistry

Valence-state distributions in the ruthenium quinonoid (L) frameworks of [Ru(trpy)(Cl)(L^1)]ClO_4 (**1**-ClO_4) and [Ru(trpy)(Cl)(L^2)]ClO_4 (**2**-ClO_4) (L^1 = *o*-iminobenzoquinone, L^2 = *o*-diiminobenzoquinone, and trpy = 2,2′:6′,2′′-terpyridine) have been examined by structural, spectroelectrochemical, and density functional studies. The structural data, in corroboration with the DFT-calculated bond lengths, suggest that the primary valence formulation of $\mathbf{1}^+$ and $\mathbf{2}^+$ is a spin-coupled singlet configuration of [Ru^{III}(trpy)(Cl)(L_{Sq})]$^+$ with a minority contribution from diamagnetic [Ru^{II}(trpy)(Cl)(L_Q)]$^+$. Consequently, the closely spaced successive two oxidation processes of $\mathbf{1}^+$ and $\mathbf{2}^+$ can be assigned to $Ru^{III} \rightarrow Ru^{IV}$ and $L_{Sq} \rightarrow L_Q$, which involve the HOMO and HOMO–3 levels, respectively. The one-electron-oxidized species $\mathbf{1}^{2+}$ and $\mathbf{2}^{2+}$ display sharp EPR signals with *g* values of 2.011 and 2.014 at 77 K, respectively. The free radical EPR signal ($g \approx 2.0$) of the one-electron-reduced species **1** or **2** signifies the preferential involvement of the ruthenium-based orbitals in the first reduction process to yield [Ru^{II}(trpy)(Cl)(L_{Sq})], although the LUMO is calculated to be a mixture of dπ(Ru) (≈24 %) and π*(L) (≈ 70 %). The subsequent second ($\mathbf{1}^-/\mathbf{2}^-$) and third ($\mathbf{1}^{2-}/\mathbf{2}^{2-}$) reduction steps in each case are associated simply with the terpyridyl-based orbitals (≥90 %). The lowest energy charge-transfer transitions of $\mathbf{1}^+$ and $\mathbf{2}^+$ at 556 and 509 nm are predicted to be HOMO → LUMO+1 and HOMO–1 → LUMO+1 transitions, respectively. In the successive oxidations $\mathbf{1}^+/\mathbf{2}^+ \rightarrow \mathbf{1}^{2+}/\mathbf{2}^{2+} \rightarrow \mathbf{1}^{3+}/\mathbf{2}^{3+}$ the lowest energy charge-transfer transitions undergo a blue shift with a substantial reduction in intensity. The lowest energy charge-transfer transitions, however, are red shifted with a reduction in intensity on going from ($\mathbf{1}^+/\mathbf{2}^+$) to **1/2**. The origin of the transitions in the $\mathbf{1}^{2+}/\mathbf{2}^{2+}$ and **1/2** systems is predicted by TDDFT analysis.

(© Wiley-VCH Verlag GmbH & Co. KGaA, 69451 Weinheim, Germany, 2007)

Introduction

The ground-state formulation of a particular mononuclear quinonoid system [(AL)Ru^n–L^{m+}] ["*n*" and "*m*" are the formal charges associated with the electronic states of the metal and quinonoid ligand (L)] can either be any of the possible valence-localized tautomeric forms, [(AL)Ru^{II}–$L°_Q$] ↔ [(AL)Ru^{III}–$L^{\cdot-}_{Sq}$] ↔ [(AL)Ru^{IV}–L^{2-}_{Cat}] or a mixed M(dπ)-L(pπ) delocalized situation depending on the electronic aspects of all the associated entities (Ru^n, L^m and AL) in the complex frameworks (Cat = fully reduced dianionic catecholate form; Sq = intermediate monoanionic radical form; Q = fully oxidized quinine form, Scheme 1; AL = ancillary ligands). The remarkable mixing of redox-facile-metal-ion- and ligand-based frontier orbitals in the ruthenium quinonoid (L) frameworks often introduces considerable ambiguities in assigning their precise valence configurations in the native state, as well as preferential involvement of the metal- or ligand-based orbitals in the accessible electron-transfer processes.[1,2] For example, experimental results have convincingly established the $Ru^{III}L_{Sq}$ formulation[3] of [Ru(acac)$_2$(L)] [acac$^-$ = acetylacetonate; L = iminoquinone (X = O, Y = NH) or iminothioquinone (X = S, Y = NH); Scheme 1] but subsequent theoretical studies suggest that the alternate resonance form of $Ru^{II}L_Q$ also contributes in the native state to some extent.[4] Thus, establishing the primary contributing electronic forms of the metal ion and L in such complexes is a formidable challenge. Although a wide variety of mononuclear ruthenium-*o*-quinonoid systems have been scrutinized over the past years, the complexities vary substantially from one molecule to another depending on the nature of X and Y in the quinonoid (L) framework (Scheme 1) and the electronic nature of the ancillary ligands (AL) associated with the complex moieties. For instance, distinct localized {$Ru^{II}L_{Cat}$} and {$Ru^{II}L_{Sq}$} configurations have been stabilized in [(tap)$_2$RuL][5] [tap = 2-(*m*-tolylazo)pyridine] and [(PPh_3)$_2$$RuL_2$],[6]

[a] Department of Chemistry, Indian Institute of Technology, Bombay,
Powai, Mumbai 400076, India
E-mail: lahiri@chem.iitb.ac.in

Supporting information for this article is available on the WWW under http://www.eurjic.org or from the author.

© 2007 Wiley-VCH Verlag GmbH & Co. KGaA, Weinheim

respectively, although the $[(bpy)_2RuL]^+$ (bpy = 2,2′-bipyridine) and $[(t\text{Bupy})_2RuL_2]$ analogs (L = X = Y = O, Scheme 1) have been described as RuL charge-delocalized systems.[2b,2u] Similarly, the RuL valence-state features in [(Cl/OAc)(trpy)RuL] (L = X = Y = O; trpy = 2,2′:6′,2′′-terpyridine, Scheme 1) have been addressed as a resonance equilibrium between $Ru^{II}L_{Sq}$ and $Ru^{III}L_{Cat}$.[7] This unique electronic characteristic of metal quinonoids justifies their continuous experimental and theoretical explorations with newer molecules.[1,2,8] This indeed is the origin of the present work, which scrutinizes the valence-state distribution profile of {RuL} coordinated to the hitherto relatively less explored terpyridine as ancillary ligand.[7,9]

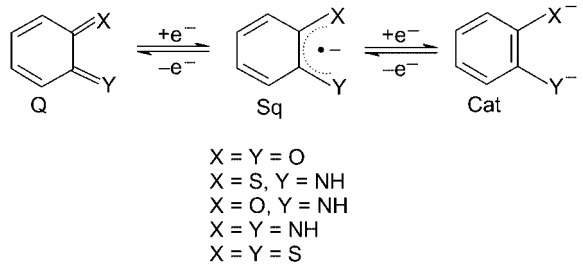

Scheme 1.

This work deals with two such conceptually simple ruthenium *o*-quinonoid species, namely $[Ru(trpy)(Cl)(L^1)]ClO_4$ (**1**-ClO_4) and $[Ru(trpy)(Cl)(L^2)]ClO_4$ (**2**-ClO_4), where L^1 and L^2 are *o*-iminobenzoquinone (X = O and Y = NH) and *o*-diiminobenzoquinone (X = Y = NH) respectively (Scheme 1). Unlike many other apparently similar systems, establishment of the {RuL} redox configurations in $\mathbf{1}^+$ and $\mathbf{2}^+$ was not as straightforward as we envisaged (see below),[3,5,6] therefore the primary objectives of the present article are to address the charge-distribution phenomena of $\{Ru^nL^m\}$ in $\mathbf{1}^+$ and $\mathbf{2}^+$ by parallel considerations of experimental results and the theoretically generated information on their optimized geometries.

Results and Discussion

The diamagnetic complexes $[Ru(trpy)(Cl)(L^1)]ClO_4$ (**1**-ClO_4) and $[Ru(trpy)(Cl)(L^2)]ClO_4$ (**2**-ClO_4) (L^1 = *o*-iminobenzoquinone and L^2 = *o*-diiminobenzoquinone; trpy = 2,2′:6′,2′′-terpyridine) were prepared by the reaction of $[RuCl_3(trpy)]$ with *o*-aminophenol and *o*-phenylenediamine, respectively, in the presence of NEt_3 as a base, in refluxing ethanol, followed by chromatographic purification on a neutral alumina column.

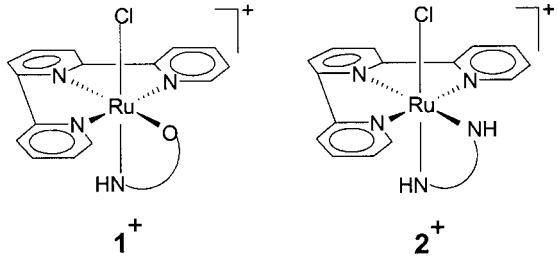

The unsymmetrical L^1 in combination with the meridional configuration of trpy in $\mathbf{1}^+$ is expected to give rise to an isomeric mixture of **A** and **B**. However, the preferential crystallization of isomer **B** was confirmed by its crystal structure (see below).

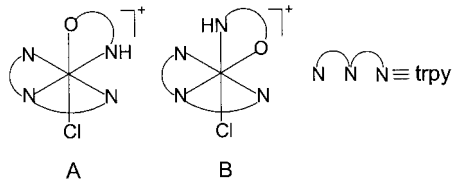

Complexes **1**-ClO_4 and **2**-ClO_4 are 1:1 conductors in acetonitrile and exhibit satisfactory microanalytical data (see Exp. Sect.). The positive-ion electrospray mass spectra show molecular ion peaks at 476.90 and 475.85 (Figure S1, Supporting Information) for $\mathbf{1}^+$ (calcd.: 477.00) and $\mathbf{2}^+$ (calcd.: 475.92), respectively. The presence of the ClO_4^- counteranion was confirmed by the appearance of characteristic $\nu(ClO_4^-)$ frequencies at 1100 and 630 cm^{-1} in their IR spectra; the NH vibrations appear near 3300 cm^{-1} (see Exp. Sect.). The ^1H NMR spectra of $\mathbf{1}^+$ and $\mathbf{2}^+$ exhibit the expected fifteen (eleven from trpy and four from L^1 or L^2), although partially overlapping, aromatic signals. The D_2O exchangeable one and two NH proton signals of coordinated L^1 and L^2 in $\mathbf{1}^+$ and $\mathbf{2}^+$, respectively, are observed in the downfield region (Figure S2, Supporting Information; see Exp. Sect.).[10] The synthesis of **2**-ClO_4 by a different synthetic route and its electronic spectrum [in H_2O; λ_{max} (ε) = 506 nm (16000 $M^{-1}cm^{-1}$), 316 (22000), 280 (20000), 274 (21000), 232 (28000)] and metal oxidation potential (0.96 V vs. Ag/AgCl in CH_3CN) have been reported earlier.[11]

The structures of **1**-ClO_4 and **2**-ClO_4 were authenticated by their single-crystal X-ray structures (Figures 1 and 2, respectively, and Table 1). The geometrical constraint that arises due to the usual meridional mode of the tridentate trpy ligand is reflected in the *trans* angles (Table 1).[12,13] The chloride is preferentially *trans* to N1H in $\mathbf{1}^+$ (structural form **B**). As a consequence of the small bite angle involving the coordinated ligand L^1 [N1–Ru–O1 78.1(3)°] or L^2 [N1–Ru–N5 78.0(3)°], the N1–Ru–Cl *trans* angle is tilted by about 10°. The Ru–Cl and Ru–N(trpy) bond lengths and the associated angles are in good agreement with the data reported for related molecules.[12–14] The Ru–N distances involving L^1 [1.942(8) Å] and L^2 [1.985(6) and 1.991(7) Å] are appreciably shorter than the corresponding Ru–N(trpy) distances (2.022 Å in $\mathbf{1}^+$ and 2.043 Å in $\mathbf{2}^+$; Table 1), which implies significant mixing of dπ(Ru) and π* of L in the respective LUMOs (see below).[15]

The C1–O1 and C6–N1H bond lengths pertaining to L^1 in $\mathbf{1}^+$ are 1.270(11) and 1.312(12) Å, respectively [C–O/C–NH distances to individual localized oxidation states (Sq and Q) are 1.30/1.35 and 1.22/1.31 Å, respectively, based on hundreds of structure of *o*-quinonoid molecules determined since 1985[8b]]. This, together with the two short C–C intraring distances in L^1 [C2–C3 1.322(13) and C4–C5 1.377(14) Å], suggests that $\mathbf{1}^+$ is primarily in a $\{Ru^{III}–Sq\}$ state, with a minor contribution from the alternate reso-

 © 2007 Wiley-VCH Verlag GmbH & Co. KGaA, Weinheim

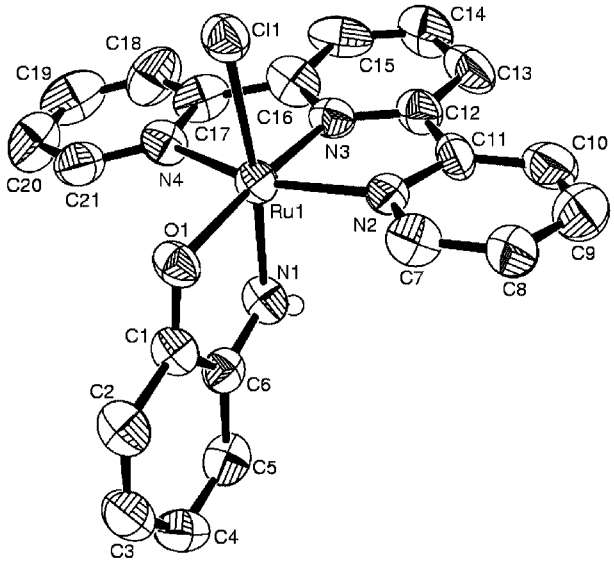

Figure 1. Crystal structure of the cation of **1**-ClO_4. Ellipsoids are drawn at the 50% probability.

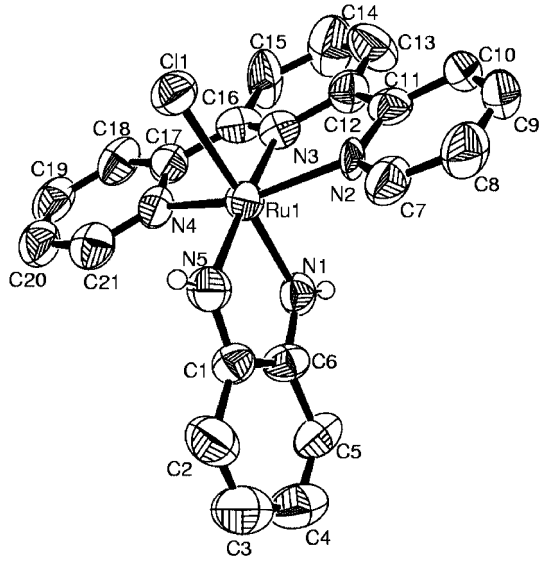

Figure 2. Crystal structure of the cation of **2**-ClO_4. Ellipsoids are drawn at the 50% probability.

nance form {Ru^{II}–Q}. On the other hand, C1–N5H, C6–N1H and the two short intra-ring bond lengths (C2–C3 and C4–C5) of L^2 in $\mathbf{2}^+$ [1.316(9), 1.317(9), 1.310(13) and 1.331(13) Å, respectively] indicate a charge-delocalized resonance form of Ru^{III}–Sq ↔ Ru^{II}–Q. Thus, the 1:1 conducting behavior and singlet (S = O) ground states of $\mathbf{1}^+$ and $\mathbf{2}^+$ can be addressed in terms of a valence tautomeric formulation of spin-coupled $[Ru^{III}(trpy)(Cl)(L_{Sq})]^+$ and diamagnetic $[Ru^{II}(trpy)(Cl)(L_Q)]^+$, as observed in $[(bpy)_2RuL]^+$ (L = X = Y = O; X = Y = NH; X = O, Y = NH).[2b,2i,7,16] However, the corresponding Ru-trpy-dioxolene derivatives [(Cl/OAc)(trpy)RuL] (L = X = Y = O, Scheme 1) are described as a resonance equilibrium between $Ru^{II}L_{Sq}$ and $Ru^{III}L_{Cat}$.[7] Hence, density functional calculations at the B3LYP level were performed for $\mathbf{1}^+$ and $\mathbf{2}^+$ in order to obtain additional structural insights from the optimized geometries.[17] In addition, geometry optimizations of the oxidized and reduced species were also performed.

The optimized geometries of $\mathbf{1}^+$ and $\mathbf{2}^+$ are shown in Figure 3, and a selected list of calculated geometric parameters is provided in Table 1 (coordinates for $\mathbf{1}^+$ and $\mathbf{2}^+$ are given in Table S1 in the Supporting Information). In general, the computed structural parameters of $\mathbf{1}^+$ and $\mathbf{2}^+$ are in reasonably good agreement with the experimental ones (Table 1). The calculated intra-ligand C–C distances of L^1 and L^2 in $\mathbf{1}^+$ and $\mathbf{2}^+$, respectively, also show two short distances (C4–

Table 1. Important experimental[a] and computed[b] bond lengths [Å] and angles [°] for **1**-ClO_4 and **2**-ClO_4.

Bond lengths					Bond angles				
	1-ClO_4		**2**-ClO_4			**1**-ClO_4		**2**-ClO_4	
	Exp.	Comp.	Exp.	Comp.		Exp.	Comp.	Exp.	Comp.
Ru1–N1	1.942(8)	1.988	1.985(6)	2.034	N1–Ru1–Cl1	170.0(2)	170.54	171.8(2)	167.87
Ru1–N2	2.068(8)	2.098	2.082(5)	2.102	N2–Ru1–Cl1	89.8(2)	86.56	87.85(17)	87.66
Ru1–N3	1.958(8)	1.976	1.980(6)	2.014	N3–Ru1–Cl1	91.9(2)	90.73	92.55(18)	91.29
Ru1–N4	2.040(8)	2.098(0.06)	2.068(6)	2.102	N4–Ru1–Cl1	89.1(2)	86.54	90.48(19)	87.66
Ru1–Cl1	2.402(3)	2.387	2.407(2)	2.400	O1–Ru1–Cl1	91.97(19)	93.19	–	–
Ru1–O1	2.053(6)	2.104	–	–	N1–Ru1–N2	93.2(3)	95.18	91.6(2)	94.77
Ru1–N5	–	–	1.991(7)	2.018	N1–Ru1–N3	98.0(3)	98.73	95.4(3)	100.84
N1–C6	1.312(12)	1.335	1.317(9)	1.329	N1–Ru1–N4	91.5(3)	95.15	93.2(2)	94.77
C1–O1	1.270(11)	1.280	–	–	N2–Ru1–N3	78.9(3)	79.27	79.8(3)	78.22
C1–C2	1.416(13)	1.427	1.401(11)	1.432	N2–Ru1–N4	158.8(3)	157.34	157.4(3)	155.85
C2–C3	1.322(13)	1.372	1.310(13)	1.367	N3–Ru1–N4	80.0(4)	79.26	77.7(3)	78.22
C3–C4	1.446(15)	1.437	1.423(15)	1.438	N1–Ru1–O1	78.1(3)	77.05	–	–
C4–C5	1.377(14)	1.369	1.331(13)	1.368	N2–Ru1–O1	99.2(3)	100.96	–	–
C5–C6	1.430(13)	1.429	1.429(11)	1.431	N3–Ru1–O1	175.7(3)	175.78	–	–
C1–C6	1.433(13)	1.462	1.419(11)	1.462	N4–Ru1–O1	102.0(3)	101.00	–	–
C1–N5	–	–	1.316(9)	1.326	N1–Ru1–N5	–	–	78.0(3)	76.62
					N2–Ru1–N5	–	–	103.3(3)	101.90
					N3–Ru1–N5	–	–	172.7(3)	177.46
					N4–Ru1–N5	–	–	99.3(3)	101.88

[a] Taken from the X-ray crystal data. [b] Calculated at the B3LYP level of theory by employing the SDD basis set for Ru and 6-31G* for all other atoms.

 © 2007 Wiley-VCH Verlag GmbH & Co. KGaA, Weinheim

C5 1.369/1.368 and C2–C3 1.372/1.367 Å; Table 1). More importantly, the C1–O1/C6–N1H and C1–N5H–C6–N1H distances of 1.280/1.335 and 1.326/1.329 Å in $\mathbf{1}^+$ and $\mathbf{2}^+$, respectively, also suggest the charge delocalization situation of $\{Ru^{III}\text{–}Sq\} \longleftrightarrow \{Ru^{II}\text{–}Q\}$.

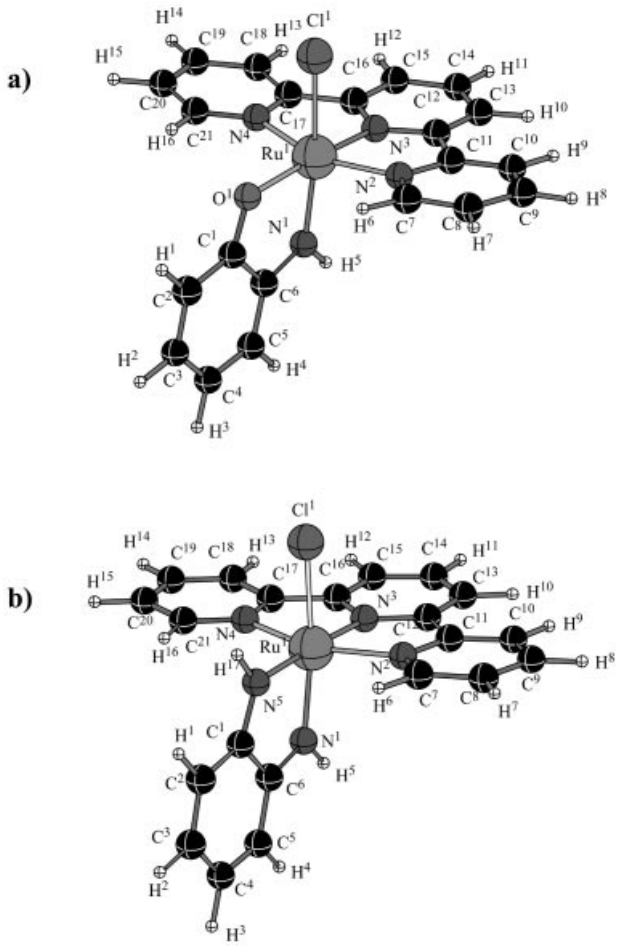

Figure 3. The B3LYP/SDD,6-31G* optimized geometries for the singlet ground state of (a) $\mathbf{1}^+$ and (b) $\mathbf{2}^+$.

Thus, a combination of the experimental and calculated structural data of $\mathbf{1}^+$ and $\mathbf{2}^+$ provide justification for the preferential ground-state formulation of $[Ru^{III}(trpy)(Cl)(L_{Sq})]^+$, with a minority contribution from $[Ru^{II}(trpy)(Cl)(L_Q)]^+$.

Both $\mathbf{1}^+$ and $\mathbf{2}^+$ show two closely spaced successive oxidation (couples I and II) and three reduction processes (couples III–V) in the potential ranges 0.94 to 1.45 and –0.26 to –1.79 V, respectively, vs. SCE (Figure 4, Table 2). The large separations in potentials between the first oxidation (couple I) and reduction (couple III) processes, ΔE = 1.45 and 1.49 V for $\mathbf{1}^+$ and $\mathbf{2}^+$, respectively, translate to comproportionation constants (K_c) of $10^{24.6}$ and $10^{25.2}$ [$RT\ln K_c = nF(\Delta E)$],[18] thereby reflecting the high stability of the native states. The more basic character of the diimine-based ligand (L^2) in $\mathbf{2}^+$ makes the first oxidation process (couple I) easier and the first reduction process (couple III) more difficult relative to iminoquinone-based L^1 in $\mathbf{1}^+$ (Table 2).[19] Although the separation in potential between couples I and II is greater in $\mathbf{2}^+$ than in $\mathbf{1}^+$, the reverse order is observed for couples III and IV, thus implying the greater and lower stabilities of the intermediate oxidized $\mathbf{2}^{2+}$ and reduced **2**, respectively, relative to the corresponding $\mathbf{1}^{2+}$ and **1**. Moreover, the irreversible profile of couples I and II for $\mathbf{1}^+$ (Figure 4a) also suggests that, unlike $\mathbf{2}^{2+/3+}$, the oxidized species $\mathbf{1}^{2+/3+}$ are not stable even on the cyclic voltammetric timescale. The relatively higher energy HOMO of complex $\mathbf{2}^+$ also points to its easier oxidation than complex $\mathbf{1}^+$ (Figure 5, Table 3). The presence of the semiquinone form of $L^{\cdot-}$ along with the anionic Cl^- in $\mathbf{1}^+$ and $\mathbf{2}^+$ makes the Ru^{III}–Ru^{II} potential substantially negative (approx. –0.3 V, see below), which, in turn, facilitates the stabilization of the Ru^{III} state under the atmospheric reaction conditions. Since the Ru^{III} and L_{Sq} states are each susceptible to one-electron oxidation to Ru^{IV} and L_Q, respectively, couples I and II can therefore be assigned to ruthenium(III)→ruthenium(IV) and coordinated $L_{Sq}\rightarrow L_Q$ processes, respectively, or vice versa.[20] The correspondence of couples I and II with metal- ($Ru^{III}\rightarrow Ru^{IV}$) and ligand-based ($L_{Sq}\rightarrow L_Q$) processes is supported by the fact that the HOMOs of $\mathbf{1}^+$

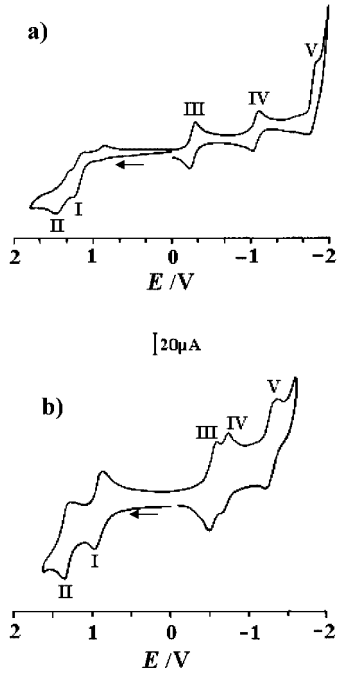

Figure 4. Cyclic voltammograms of a 10^{-3} M solution of (a) (**1**-ClO_4) and (b) (**2**-ClO_4) in CH_3CN/0.1 M Et_4NClO_4 at 298 K (scan rate: 50 mV s^{-1}).

Table 2. Redox potentials[a,b] of the complexes.

	Couple I	II	III	IV	V
1-ClO_4	1.26[c]	1.45[c]	–0.26 (90)	–1.07 (80)	–1.79 (100)
2-ClO_4	0.94 (70)	1.32 (90)	–0.54 (70)	–0.70 (60)	–1.27 (140)

[a] Potentials $E°_{298}$ [V] (ΔE [mV]) vs. SCE. [b] In CH_3CN/0.1 M Et_4NClO_4. [c] E_{pa} is considered due to the irreversible nature of the voltammograms.

 © 2007 Wiley-VCH Verlag GmbH & Co. KGaA, Weinheim

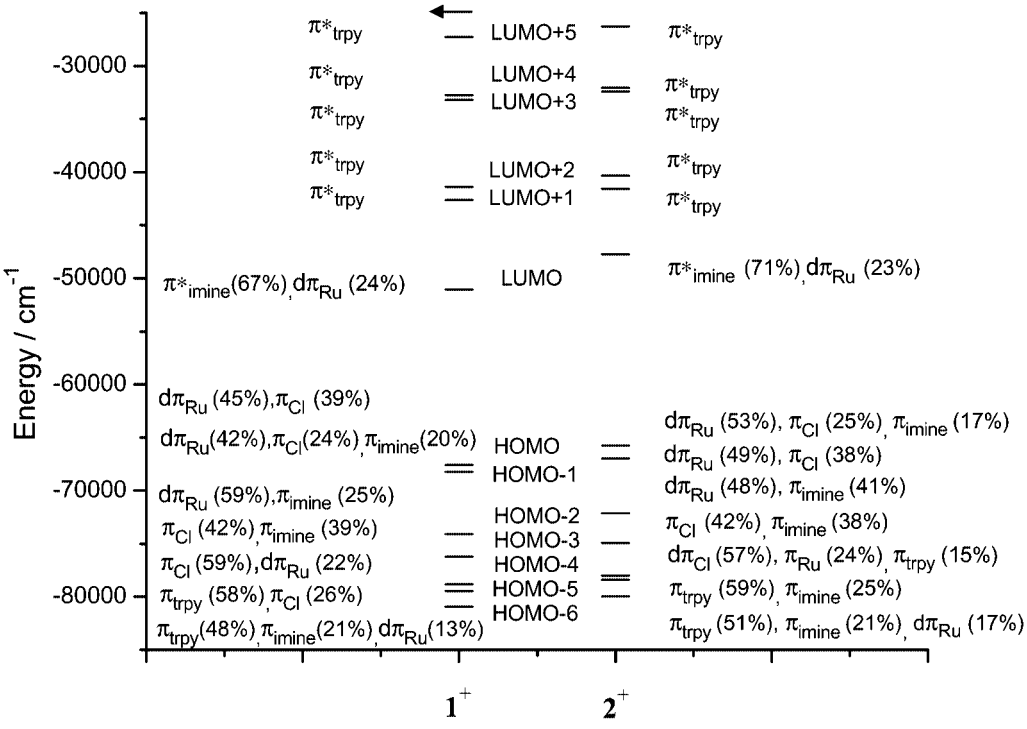

Figure 5. Orbital energy diagrams for $\mathbf{1}^+$ and $\mathbf{2}^+$ computed at the B3LYP/SDD,6-31G* level of theory.

and $\mathbf{2}^+$consist of 45% and 53% of dπ(Ru) with zero and 17% contributions from π(L^1) and π(L^2), respectively, and the HOMO–3s are dominated by π(L^1) (39%) and π(L^2) (38%), with slight metal contributions of 5.7% and 11% for $\mathbf{1}^+$ and $\mathbf{2}^+$, respectively (Figure 5, Table 3). The electrochemically generated one-electron-oxidized Ru^{IV}–L_{Sq} states in $\mathbf{1}^{2+}$ and $\mathbf{2}^{2+}$ exhibit free radical EPR signals in CH_3CN with *g* values of 2.011 (peak-to-peak separation: 18 G) and 2.014 (peak-to-peak separation: 15 G), respectively.

The DFT results also suggest that the mixing of π(L^2) and dπ(Ru) orbitals at both the HOMO and HOMO–3 levels is more pronounced in $\mathbf{2}^+$.[15,21] It is interesting to note that HOMO and HOMO–3 exhibit a fairly good mixing with chloride π orbitals (39/25% and 42% for $\mathbf{1}^+$ and $\mathbf{2}^+$, respectively), as observed in the analogous isomeric ruthenium terpyridine complexes [Ru(trpy)(Cl){3-amino-6-(3,5-dimethylpyrazol-1-yl)-1,2,4,5-tetrazine}].[13]

The observed Ru- and L-based successive two-step oxidation processes (couples I and II) in $\mathbf{1}^+$ and $\mathbf{2}^+$ also support their primary valence-state composition of $\{Ru^{III}–L_{Sq}\}$ in solution instead of the alternate possible formulation of $\{Ru^{II}–L_Q\}^+$ in which only a ruthenium-based oxidation process is expected due to the fully oxidized nature of L_Q. Similarly, the first reduction (couple III) could either be associated with the ruthenium(III) or L_{Sq} center as both are susceptible to one-electron reduction and the resultant reduced species (**1/2**) would then be formulated as $[Ru^{III}(trpy)(Cl)(L_{Sq})]^+$ ($\mathbf{1}^+/\mathbf{2}^+$) + $e^- \rightarrow [Ru^{II}(trpy)(Cl)(L_{Sq})]$ or $[Ru^{III}(trpy)(Cl)(L_{Cat})]$ (**1/2**), leaving the unpaired spin predominantly on the L_{Sq} or Ru^{III}. The semiquinone-based free radical EPR signals (*g* = 2.0023 and 2.0051, with peak-to-peak separations of 17 and 20 G for **1** and **2**, respectively;[22] see Figure 6), however, suggest a preferential metal-based reduction process to form $[Ru^{II}(trpy)(Cl)(L_{Sq})]$. The separation in potentials of approximately 1.5 V between the first oxidation (couple I) and reduction (couple III) processes in $\mathbf{1}^+$ and $\mathbf{2}^+$ also matches well with the earlier observed ruthenium-based average potential difference of about 1.5 V between the $Ru^{IV/III}$ and $Ru^{III/II}$ couples.[23]

Table 3. Orbital energies and atomic orbital contribution of frontier molecular orbitals of $\mathbf{1}^+$ and $\mathbf{2}^+$ computed at the B3LYP level of theory by employing the SDD basis set for Ru and 6-31G* for all other atoms.

MO	Energy (eV)	% Ru	% Cl	% imine (L^1/L^2)	% trpy
$\mathbf{1}^+$	LUMO – HOMO = 2.05 eV (16528 cm^{-1})				
LUMO+2	–5.13 (–41380)[a]	2.1	0.0	0.0	96.5
LUMO+1	–5.29 (–42638)	7.4	0.0	0.0	89.6
LUMO	–6.33 (–51056)	24.4	0.0	66.3	4.7
HOMO	–8.38 (–67585)	44.6	38.5	0.0	7.3
HOMO–1	–8.46 (–68224)	42.2	23.8	19.6	0.0
HOMO–2	–9.18 (–74079)	59.0	0.0	24.6	4.0
HOMO–3	–9.45 (–76213)	5.7	41.9	39.0	3.2
$\mathbf{2}^+$	LUMO – HOMO = 2.24 eV (18028 cm^{-1})				
LUMO+2	–5.00 (–40351)	2.2	0.0	0.6	97.2
LUMO+1	–5.16(–41582)	7.0	1.2	0.8	91.0
LUMO	–5.92 (–47734)	23.0	1.26	70.5	5.3
HOMO	–8.15 (–65762)	52.6	24.5	16.6	6.3
HOMO–1	–8.30 (–66973)	49.3	37.5	3.1	10.0
HOMO–2	–8.94 (–72116)	47.7	5.8	40.7	5.8
HOMO–3	–9.29 (–74951)	10.8	41.6	38.2	9.5

[a] Values in parentheses are orbital energies [cm^{-1}].

While the EPR results are strongly in favor of a metal-based reduction, the participation of Ru orbitals in the

 © 2007 Wiley-VCH Verlag GmbH & Co. KGaA, Weinheim

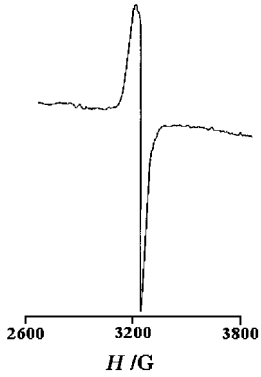

Figure 6. EPR spectrum of **1** in CH_3CN/Et_4NClO_4 at 77 K. The expected nitrogen hyperfine lines cannot be resolved at 77 K.

LUMOs is predicted to be lower than that of L_{Sq}. The contributions of Ru/L_{Sq} orbitals to the LUMOs are found to be 24/66% and 23/70%, respectively, for $\mathbf{1}^+$ and $\mathbf{2}^+$ (Figure 5, Table 3). Hence, a comparatively lower, but still significant, metal contribution favors the metal-centered reduction process in a mixed Ru(dπ)/L(π*) situation.[21] The subsequent higher energy unoccupied MOs such as LUMO+1 and LUMO+2 are primarily localized on the trpy ligand with a composition of >90% π*(trpy) orbitals along with a slight metal contribution (2–7%), which implies that the second (couple IV) and third (couple V) reductions are trpy-based (Figure 4, Table 2).[24]

In order to get further insights into the reduced species the spin densities[25] for one-electron-reduced species **1** and **2** were computed at the same level of theory. The results are in accordance with the nature of the LUMOs described earlier. The overall spin density of the complexes was found to be distributed over the metal and L^1/L^2, thus supporting an "Sq" formalism for the reduced species (Figure S3, Supporting Information). It is also worth mentioning that the contribution of the trpy ligand to the first reduction process is negligible.

Natural population analysis (NPA) for $\mathbf{1}^+$ and $\mathbf{2}^+$ at the B3LYP/SDD,6-31G* level[8c,26] suggest a d-orbital population of 6.98 and 7.03 electrons for $\mathbf{1}^+$ and $\mathbf{2}^+$, respectively (Table 4). The extra population of about $2e^-$ is expected to be an effect of charge transfer from the anionic forms of the ligands (Cl^- is a $2e^-$ donor and $L^{\cdot -}_{Sq}$ a $1e^-$ donor). The d-electron population further indicates a relatively high electron density for $\mathbf{2}^+$, in agreement with its easier oxidation than $\mathbf{1}^+$ (Table 2, Figures 4 and 5).

Table 4. Valence shell electron population of the Ru centers in $\mathbf{1}^+$ and $\mathbf{2}^+$ computed at the B3LYP/SDD, 6-31G* level.

Complex	Valence shell population	
	5s	4d
$\mathbf{1}^+$	0.30	6.98
$\mathbf{2}^+$	0.30	7.03

Both $\mathbf{1}^+$ and $\mathbf{2}^+$ display multiple charge-transfer transitions in the visible region in addition to intense ligand-based bands in the UV region (Figure 7, see Exp. Sect.). Selected computed vertical excitation energies with the TD-DFT/B3LYP formalism for the B3LYP/SDD,6-31G* geometries of $\mathbf{1}^+$ and $\mathbf{2}^+$ in their singlet ground states are summarized in Table 5 (complete lists are given in Tables S2 and S3 in the Supporting Information).[27] A comparison between the observed and computed transitions was performed by examining the transitions of comparable intensities guided by their respective oscillator strengths and absorptivity values.[28] The nature of the excited states is assigned based on the percent Kohn–Sham orbital contributions of the orbitals involved in the electronic transitions. Based on the predicted values for the oscillator strengths it is found that the most intense long-wavelength transition at 556 nm (calcd.: 522 nm) for $\mathbf{1}^+$ is from the HOMO [dπ(Ru) (45%) and π(Cl) (39%)] to the LUMO+1 [π*(trpy) (90%)] (Figure 8, a). The other two closely spaced higher energy transitions at 483 and 459 nm (calcd.: 482 and 458 nm) are due to HOMO–3→LUMO/HOMO–1→LUMO+2 and HOMO→LUMO+2 transitions, respectively (Table 5, Figure 8, a).

Similarly, the lowest energy charge-transfer band for $\mathbf{2}^+$ appears at 509 nm, which is very much in agreement with

Table 5. Singlet excitation energies computed for $\mathbf{1}^+$ and $\mathbf{2}^+$at the B3LYP level of theory.[a]

Excitation energy[b] (10^3 cm^{-1})	Oscillator strength	ε[c]	ψ_o–ψ_v [d]	Type of transition
$\mathbf{1}^+$				
19.167 (521.70)	0.1172	8230.6278	HOMO→LUMO+1 (0.59)[e]	$d\pi_{Ru}$, $\pi_{Cl}\rightarrow\pi^*_{trpy}$
(exp. 556)		(exp. 19790)		
20.751 (481.91)	0.0966	6783.9475	HOMO–3→LUMO (0.45)	π_{Cl}, $\pi_{imine}\rightarrow\pi^*_{imine}$, $d\pi_{Ru}$
(exp. 483)		(exp. 10400)	HOMO–1→LUMO+2 (0.41)	$d\pi_{Ru}$, π_{Cl}, $\pi_{imine}\rightarrow\pi^*_{trpy}$
21.838 (457.92)	0.0611	4290.8819	HOMO→LUMO +2 (0.47)	$d\pi_{Ru}$, $\pi_{Cl}\rightarrow\pi^*_{trpy}$
(exp. 459)		(exp. 8200)		
$\mathbf{2}^+$				
20.243 (493.98)	0.1098	7710.9465	HOMO–1→LUMO+1 (0.47)	$d\pi_{Ru}$, $\pi_{Cl}\rightarrow\pi^*_{trpy}$
(exp.509)		(exp. 15670)		
21.828 (458.13)	0.0364	2556.2700	HOMO–3→LUMO (0.54)	π_{Cl}, π_{imine}, $d\pi_{Ru}\rightarrow\pi^*_{imine}$, $d\pi_{Ru}$
23.557 (424.51)	0.2341	16440.1870	HOMO–3→LUMO (0.33)	π_{Cl}, π_{imine}, $d\pi_{Ru}\rightarrow\pi^*_{imine}$, $d\pi_{Ru}$

[a] Calculations were done by employing the SDD basis set for Ru and 6-31G* for all other elements. [b] Singlet excitation energies. Energy values [nm] given in parentheses. [c] ε [$M^{-1}cm^{-1}$]. [d] Occupied and virtual orbitals. [e] Transition coefficients.

 © 2007 Wiley-VCH Verlag GmbH & Co. KGaA, Weinheim

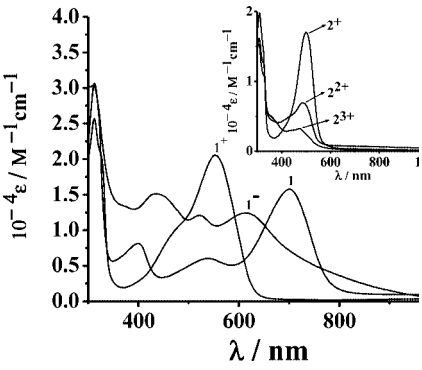

Figure 7. Electronic spectra of $\mathbf{1}^+$, **1**, and $\mathbf{1}^-$ in CH_3CN/Et_4NClO_4. The inset shows the electronic spectra of $\mathbf{2}^+$, **2**, and $\mathbf{2}^{2+}$ in CH_3CN/Et_4NClO_4.

the calculated value of 494 nm, and is due to a HOMO–1 [dπ(Ru) (49%) and π(Cl) (38%)]→LUMO+1 [π*(trpy) (91%)] transition, which is again a MLLCT transition as in $\mathbf{1}^+$. The other two closely spaced predicted transitions at 458 and 425 nm (HOMO–3→LUMO; Figure 8 (b), Table 5) could not be resolved experimentally.

On electrochemical successive oxidations of $\mathbf{1}^+$ to $\mathbf{1}^{2+}$ and $\mathbf{1}^{3+}$ and $\mathbf{2}^+$ to $\mathbf{2}^{2+}$ and $\mathbf{2}^{3+}$ the lowest energy charge-transfer bands are blue shifted from 556 to 475 and 436 nm and 509 to 487 and 476 nm, respectively, with a substantial reduction in intensity [Figure 7 (inset); see Exp. Sect.], thus indicating a lower degree of delocalization in the oxidized states. The predicted transitions for $\mathbf{1}^{2+}$ and $\mathbf{2}^{2+}$, respectively, are 491 nm [HOMO–3 {π(L^1), dπ(Ru)}→LUMO+1 {π*(L^1), dπ(Ru)}] and 465 nm [HOMO–3 {π(Cl), π(L^2), dπ(Ru)}→LUMO {π*(L^2)}] (Table S4).

During the one-electron reduction $\mathbf{1}^+ \rightarrow \mathbf{1}$ the lowest energy charge-transfer band undergoes a substantial red shift from 556 to 702 nm with a slight decrease in intensity that suggests a comparable extent of delocalization in both states. However, on further reduction to $\mathbf{1}^-$ the bands are blue shifted and undergo a reasonable intensity reduction, which implies a relatively localized state (Figure 7 and Exp. Sect.). Similar spectral features have also been observed with **2** and $\mathbf{2}^-$ (see Exp. Sect.).[4c,4d] TD-DFT calculations on the reduced species indicate that during the one electron reductions $[\mathbf{1}]^+ \rightarrow \mathbf{1}$ and $[\mathbf{2}]^+ \rightarrow \mathbf{2}$, the lowest energy charge transfer (MLLCT) bands undergo a red shift to 604 and 556 nm, respectively. These bands are predicted to have contributions from intra-ligand transitions as well, namely HOMO–2 [dπ(Ru) (58%), π(L^1) (32%)]→LUMO [π*(L^1) (48%), π*(trpy) (44%)] and HOMO–2 [dπ(Ru) (55%), π(L^2) (32%)]→LUMO [π*(L^2) (7%), π*(trpy) (91%)], respectively (Table S4). The deviation of the predicted value from the experimental one might be due to the absence of solvent effects in our calculations.

The frontier orbital analysis further indicates that the nature of the HOMOs and LUMOs remains essentially the same after oxidation. For instance, the composition of the HOMO changes only from 45% (Ru) and 39% (Cl) in $\mathbf{1}^+$ to 43% (Ru) and 46% (Cl) in $\mathbf{1}^{2+}$ upon oxidation, whereas the contribution of the ligand orbital to the frontier orbitals

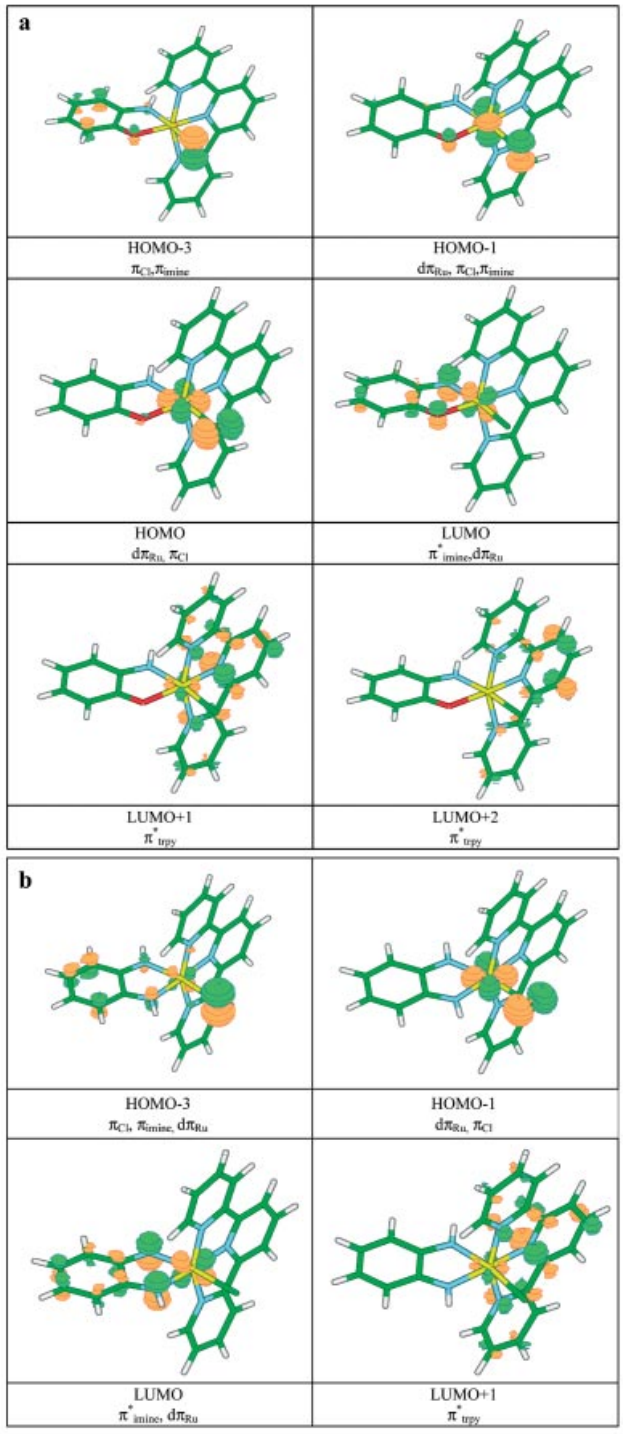

Figure 8. a) Kohn–Sham orbital contours of the frontier MOs of $\mathbf{1}^+$ involved in the intense long-wavelength transitions. b) Kohn–Sham orbital contours of the frontier MOs of $\mathbf{2}^+$ involved in the intense long-wavelength transitions.

increases to a greater extent upon reduction to **1**. The LUMO becomes primarily ligand centered and is composed mainly of L^1- (48%) and trpy-based (44%) orbitals along with less than 10% Ru contribution. However, the HOMOs are essentially dominated by L — the Ru/L contributions

 © 2007 Wiley-VCH Verlag GmbH & Co. KGaA, Weinheim

are 19/74 and 18/77%, respectively, for **1** and **2** (Tables S5 and S6).

It should be noted that the experimental results reported for similar molecules $[Ru^{III}(acac)_2(L_{Sq})]$ ($acac^-$ = acetylacetonate; L corresponds to X = O, Y = NH/X = S, Y = NH, Scheme 1) established the preferential involvement of L_{Sq} in the oxidation and reduction processes, which leaves the unpaired spin on the ruthenium(III) ion.[3] However, the DFT-supported experimental results for the present molecules $\mathbf{1}^+$ and $\mathbf{2}^+$ demonstrate a metal-based first oxidation and first reduction, which leaves the resultant spin on the ligand center (L). Thus, the present study further emphasizes that ruthenium quinonoid systems of apparently similar chemical structures may exhibit substantial variations in their electronic features both in native and accessible redox states, which indeed justifies the need for further critical explorations with the newer molecular frameworks.

In conclusion, a combination of experimental and DFT results suggests the following: (i) the ground-state valence formulation of $[Ru(trpy)(Cl)(L^{1/2})]^+$ ($\mathbf{1}^+/\mathbf{2}^+$) can be best interpreted as spin-coupled Ru^{III}–L_{Sq} in combination with a minority contribution from diamagnetic Ru^{II}–L_Q; (ii) the involvement of dπ(Ru)- and π(L)-based frontier orbitals, respectively, in the successive oxidation processes (couples I and II); (iii) the preferential involvement of Ru-based orbitals in the first reduction step (couple III), although the LUMO is calculated to be a mixture of dπ(Ru) (≈ 24%) and π*(L) (≈ 70%) orbitals; (iv) the primary participation of π*(trpy) orbitals in the subsequent second and third reductions (couples IV and V).

Experimental Section

Materials and Instrumentation: The precursor complex $[Ru(trpy)Cl_3]$ was prepared according to the reported procedure.[29] 2,2′:6′,2′′-Terpyridine (trpy), *o*-aminophenol and *o*-phenylenediamine were procured from Aldrich, USA. Other chemicals and solvents were reagent grade and used as received. HPLC-grade solvents were used for spectroscopic and electrochemical studies.

UV/Vis spectral studies were performed with a Perkin–Elmer Lambda-950 spectrophotometer. FT-IR spectra were recorded with a Nicolet spectrophotometer with samples prepared as KBr pellets. Solution electrical conductivity was checked using a Systronic 305 conductivity bridge. ^{1}H NMR spectra were obtained with a 400 MHz Varian FT spectrometer. The EPR measurements were performed with a Varian model 109C E-line X-band spectrometer fitted with a quartz dewar for measurements at 77 K. Cyclic voltammetric, differential pulse voltammetric, and coulometric measurements were carried out using a PAR model 273A electrochemistry system. Platinum wire working and auxiliary electrodes and an aqueous saturated calomel reference electrode (SCE) were used in a three-electrode configuration. The supporting electrolyte was Et_4NClO_4 and the solute concentration was around 10^{-3} M. The half-wave potential, $E°_{298}$, was set equal to $0.5(E_{pa} + E_{pc})$, where E_{pa} and E_{pc} are the anodic and cathodic cyclic voltammetric peak potentials, respectively. A platinum wire-gauze working electrode was used in coulometric experiments. All measurements were carried out under dinitrogen. The magnetic susceptibility was measured with a Faraday balance (CAHN Instruments Inc.; Serial no. 76240). Electrospray mass spectra were recorded with a Micromass Q-ToF mass spectrometer.

$[Ru(trpy)(Cl)(L^1)]ClO_4$ (1-ClO_4) and $[Ru(trpy)(Cl)(L^2)]ClO_4$ (2-ClO_4): These complexes were prepared by following the same general procedure. $[Ru(trpy)Cl_3]$ (100 mg, 0.226 mmol), *o*-aminophenol (24 mg, 0.220 mmol) or *o*-phenylenediamine (25 mg, 0.226 mmol), and NEt_3 (0.4 mL, 2.86 mmol) were taken in 20 mL of ethanol and the mixture was heated at reflux for 5 h under atmospheric conditions. The initial dark brown color changed to purple or red. The solvent of the reaction mixture was evaporated to dryness under reduced pressure. The solid mass thus obtained was dissolved in a minimum volume (5 mL) of CH_3CN/CH_3OH (4:1) and reprecipitated by addition of a saturated aqueous solution of $NaClO_4$. The dark precipitate was filtered off and washed thoroughly with ice-cold water. The product was dried in vacuo over P_4O_{10}. It was then purified on an alumina (neutral) column. The purple or red product was eluted with CH_2Cl_2/CH_3CN (1:1). Evaporation of the solvent under reduced pressure afforded the pure complexes.

1-ClO_4: Yield: 55 mg (42%). $C_{21}H_{16}Cl_2N_4O_5Ru$: calcd. C 43.73, H 2.80, N 9.72; found C 43.56, H 2.87, N 9.51. Molar conductivity in acetonitrile: Λ_M = 110 $\Omega^{-1}cm^2M^{-1}$. ^{1}H NMR [400 MHz, $(CD_3)_2SO$, 298 K]: δ = 15.31 (s, 1 H, NH), 8.85 (d, J = 7.6 Hz, 2 H), 8.72 (d, J = 7.6 Hz, 2 H), 8.34 (t, J = 8.4, 8.0 Hz, 1 H), 8.16 (m, 3 H), 7.89 (d, J = 9.2 Hz, 1 H), 7.54 (t, J = 6.4, 6.0 Hz, 2 H), 7.43 (d, J = 5.6 Hz, 2 H), 7.27 (d, J = 8.8 Hz, 1 H), 7.02 ppm (t, J = 6.4, 7.2 Hz, 1 H). UV/Vis (acetonitrile): λ_{max} (ε) = 556 nm (19790 $M^{-1}cm^{-1}$), 483 (10400), 459 (8200), 311 (24630), 270 (24910), 232 (35280). IR (KBr disk): ν(ClO_4^-) = 1086/624 cm^{-1}; ν(NH) = 3217.

$\mathbf{1}^{2+}$: UV/Vis (acetonitrile/0.1 M Et_4NClO_4): λ_{max} (ε) = 475 nm (3900 $M^{-1}cm^{-1}$), 438 (4500), 324 (17400), 308 (19600), 232 (29400).

$\mathbf{1}^{3+}$: UV/Vis (acetonitrile/0.1 M Et_4NClO_4): λ_{max} (ε) = 436 nm (3100 $M^{-1}cm^{-1}$), 332 (12700), 318 (14600), 285 (19400), 273 (19900).

1: UV/Vis (acetonitrile/0.1 M Et_4NClO_4): λ_{max} (ε) = 702 nm (15380 $M^{-1}cm^{-1}$), 537 (5980), 399 (7920), 311 (29460), 277 (28090), 235 (47020).

$\mathbf{1}^-$: UV/Vis (acetonitrile/0.1 M Et_4NClO_4): λ_{max} (ε) = 615 nm (12020 $M^{-1}cm^{-1}$), 521 (11720), 436 (14650), 311 (29020).

2-ClO_4: Yield: 40 mg (30%). $C_{21}H_{17}Cl_2N_5O_4Ru$: calcd. C 43.84, H 2.98, N 12.17; found C 44.19, H 2.75, N 11.99. Molar conductivity in acetonitrile: Λ_M = 140 $\Omega^{-1}cm^2M^{-1}$. ^{1}H NMR [400 MHz, $(CD_3)_2SO$, 298 K]: δ = 14.36 (s, NH), 11.91 (s, NH), 8.90 (d, J = 8.4 Hz, 2 H), 8.72 (d, J = 8.4 Hz, 2 H), 8.41 (t, J = 8.0 Hz, 1 H), 8.07 (t, J = 6.4, 8.0 Hz, 2 H), 7.76 (d, J = 8.8 Hz, 1 H), 7.44 (t, J = 6.8, 6.4 Hz, 2 H), 7.38 (d, J = 5.6 Hz, 2 H), 7.07 (t, J = 5.2, 6.0 Hz, 1 H), 6.93 ppm (d, J = 5.6 Hz, 2 H). UV/Vis (acetonitrile): λ_{max} (ε) = 509 nm (15670 $M^{-1}cm^{-1}$), 311 (17210), 280 (16190), 269 (18330), 234 (22690), 208 (28930). IR (KBr disk): ν(ClO_4^-) = 1086/625 cm^{-1}; ν(NH) = 3317.

$\mathbf{2}^{2+}$: UV/Vis (acetonitrile/0.1 M Et_4NClO_4): λ_{max} (ε) = 487 nm (6630 $M^{-1}cm^{-1}$), 440 (5030), 327 (12070), 308 (15580), 282 (16330), 270 (17750), 232 (26300).

$\mathbf{2}^{3+}$: UV/Vis (acetonitrile/0.1 M Et_4NClO_4): λ_{max} (ε) = 476 nm (3140 $M^{-1}cm^{-1}$), 376 (4190), 327 (10640), 305 (14720), 268 (18600).

2: UV/Vis (acetonitrile/0.1 M Et_4NClO_4): λ_{max} (ε) = 718 nm (2530 $M^{-1}cm^{-1}$), 516 (4580), 477 (5140), 328 (5930), 309 (9020), 243 (20400), 204 (27000).

$\mathbf{2}^-$: UV/Vis (acetonitrile/0.1 M Et_4NClO_4): λ_{max} (ε) = 596 nm (4180 $M^{-1}cm^{-1}$), 523 (5740), 475 (7580), 439 (8840), 325 (11860), 262 (29940).

 © 2007 Wiley-VCH Verlag GmbH & Co. KGaA, Weinheim

X-ray Crystallography: Single crystals of **1**-ClO_4 and **2**-ClO_4 were grown by slow evaporation of their 1:1 acetonitrile/methanol and 1:1 acetonitrile/toluene solutions, respectively. Diffraction data for **1**-ClO_4 and **2**-ClO_4 were collected with Enraf–Nonius CAD-4 (MACH-3) and OXFORD XCALIBUR-S CCD single-crystal X-ray diffractometers, respectively. The structures were solved and refined by full-matrix least-squares techniques on F^2 using SHELX-97.[30] The absorption corrections for **1**-ClO_4 and **2**-ClO_4 were done by psi-scans and multi-scans, respectively. All the data were corrected for Lorentz and polarization effects, and the non-hydrogen atoms were refined anisotropically. Hydrogen atoms were included in the refinement process as per the riding model. See Table 6 for further details.

Table 6. Crystallographic data for **1**-ClO_4 and **2**-ClO_4.

	(**1**-ClO_4)	(**2**-ClO_4)
Formula	$C_{21}H_{16}Cl_2N_4O_5Ru$	$C_{21}H_{17}Cl_2N_5O_{4.50}Ru$
M_r	576.35	583.37
Crystal system	monoclinic	orthorhombic
Space group	*C*2/*c*	*Pbcn*
T [K]	293(2)	293(2)
λ [Å]	0.71073	0.71073
a [Å]	23.269(3)	21.126(6)
b [Å]	13.354(2)	13.379(4)
c [Å]	15.3500(12)	15.837(9)
β [°]	113.335(8)	90
V [Å^3]	4379.6(9)	4476(3)
Crystal size [mm]	$0.20\times0.15\times0.05$	$0.30\times0.25\times0.20$
$\rho_{calcd.}$ [g cm^{-3}]	1.748	1.731
Z	8	8
μ [mm^{-1}]	1.003	0.982
F (000)	2304	2336
2θ range [°]	3.60 to 49.94	6.28 to 50.00
Reflections collected	3886	31091
Unique reflections (R_{int})	3790 (0.0338)	3931 (0.0991)
Data/restraints/parameters	3790/0/298	3931/0/303
Goodness-of-fit	0.968	0.884
R_1 [$I > 2\sigma(I)$]	0.0617	0.0605
wR_2 [all data]	0.1737	0.1598
Largest diff. peak/hole, [e Å^{-3}]	0.943/–0.602	1.132/–0.454

CCDC-606479 (for **1**-ClO_4) and -606480 (for **2**-ClO_4) contain the supplementary crystallographic data for this paper. These data can be obtained free of charge from The Cambridge Crystallographic Data Centre via www.ccdc.cam.ac.uk/data_request/cif.

Computational Details: Full geometry optimizations of $\mathbf{1}^+$ and $\mathbf{2}^+$ were carried out using the density functional theory method at the (U)B3LYP level.[31a,31b] All elements except ruthenium were assigned the 6-31G* basis set. The SDD basis set with effective core potential was employed for the ruthenium atoms.[31c,31d] Calculations were performed with Gaussian 98 and Gaussian 03.[31e,31f] Vertical electronic excitations based on the B3LYP-optimized geometries were computed using the time-dependent density functional theory (TD-DFT) formalism,[31g] with the B3LYP functional using the above combination of basis sets. Natural population analysis was performed using the NBO 3.1 program package as implemented in Gaussian98.[31h,31i] The spin densities of complexes were computed using the CUBE option as implemented in Gaussian 03. Visual inspection of the key orbitals was done with MOLDEN,[31h] to assign the nature of the various electronic transitions. Molecular orbital compositions were analyzed using the AOMIX program.[31i,31j]

Supporting Information (see also the footnote on the first page of this article): Optimized coordinates (Table S1), excitation energies (Tables S2/S3/S4), MO compositions (Tables S5/S6), mass and NMR spectra (Figures S1/S2), spin densities (Figure S3), Kohn–Sham orbitals (Figures S4/S5).

Acknowledgments

Financial support received from the Department of Science and Technology and Council of Scientific and Industrial Research, New Delhi, India is gratefully acknowledged. X-ray structural studies for **1**-ClO_4 and **2**-ClO_4 were carried out at the National Single Crystal Diffractometer Facility, Indian Institute of Technology, Bombay. Special acknowledgment is made to the Sophisticated Analytical Instrument Facility (SAIF) and the Computer Center, Indian Institute of Technology, Bombay, respectively, for providing the EPR and computational facilities.

[1] a) C. G. Pierpont, C. W. Lange, *Prog. Inorg. Chem.* **1994**, *41*, 331; b) S. Kar, B. Sarkar, S. Ghumaan, D. Janardanan, J. van Slageren, J. Fiedlar, V. G. Puranik, R. B. Sunoj, W. Kaim, G. K. Lahiri, *Chem. Eur. J.* **2005**, *11*, 4901; c) A. Vlček Jr., *Comments Inorg. Chem.* **1994**, *16*, 207.

[2] a) R. B. Salmonsen, A. Abelleira, M. J. Clarke, *Inorg. Chem.* **1984**, *23*, 387; b) M. Haga, E. S. Dodsworth, A. B. P. Lever, *Inorg. Chem.* **1986**, *25*, 447; c) A. Dei, D. Gatteschi, L. Pardi, *Inorg. Chem.* **1990**, *29*, 1443; d) C. G. Pierpont, A. S. Attia, *Collect. Czech. Chem. Commun.* **2001**, *66*, 33; e) C. G. Pierpont, *Coord. Chem. Rev.* **2001**, *219–221*, 415; f) J. Rall, M. Wanner, M. Albrecht, F. M. Hornung, W. Kaim, *Chem. Eur. J.* **1999**, *5*, 2802; g) G. Speier, A. Whalen, J. Csihony, C. G. Pierpont, *Inorg. Chem.* **1995**, *34*, 1355; h) V. Kasack, W. Kaim, H. Binder, J. Jordanov, E. Roth, *Inorg. Chem.* **1995**, *34*, 1924; i) M. Ebadi, A. B. P. Lever, *Inorg. Chem.* **1999**, *38*, 467; j) C. N. Verani, S. Gallert, E. Bill, T. Weyhermüller, K. Wieghardt, P. Chaudhuri, *Chem. Commun.* **1999**, 1747; k) P. Chaudhuri, C. N. Verani, E. Bill, E. Bothe, T. Weyhermüller, K. Wieghardt, *J. Am. Chem. Soc.* **2001**, *123*, 2213; l) H. Chun, E. Bill, E. Bothe, T. Weyhermüller, K. Wieghardt, *Inorg. Chem.* **2002**, *41*, 5091; m) P. Ghosh, A. Begum, D. Herebian, E. Bothe, K. Hildenbrand, T. Weyhermüller, K. Wieghardt, *Angew. Chem. Int. Ed.* **2003**, *42*, 563; n) K. S. Min, T. Weyhermüller, K. Wieghardt, *Dalton Trans.* **2003**, 1126; o) S. Patra, B. Sarkar, S. Ghumaan, J. Fiedler, S. Zalis, W. Kaim, G. K. Lahiri, *Dalton Trans.* **2004**, 750; p) S. I. Gorelsky, A. B. P. Lever, *J. Organomet. Chem.* **2001**, *635*, 187; q) S. I. Gorelsky, E. S. Dodsworth, A. B. P. Lever, A. A. Vlcek, *Coord. Chem. Rev.* **1998**, *174*, 469; r) A. B. P. Lever, S. I. Gorelsky, *Coord. Chem. Rev.* **2000**, *208*, 153; s) C. J. Cunha, E. S. Dodsworth, M. A. Monteiro, A. B. P. Lever, *Inorg. Chem.* **1999**, *38*, 5399; t) R. A. Metcalfe, A. B. P. Lever, *Inorg. Chem.* **1997**, *36*, 4762; u) S. R. Boone, C. G. Pierpont, *Inorg. Chem.* **1987**, *26*, 1769.

[3] S. Patra, B. Sarkar, S. M. Mobin, W. Kaim, G. K. Lahiri, *Inorg. Chem.* **2003**, *42*, 6469.

[4] C. Remenyi, M. Kaupp, *J. Am. Chem. Soc.* **2005**, *127*, 11399.

[5] N. Bag, A. Pramanik, G. K. Lahiri, A. Chakravorty, *Inorg. Chem.* **1992**, *31*, 40.

[6] N. Bag, G. K. Lahiri, P. Basu, A. Chakravorty, *J. Chem. Soc., Dalton Trans.* **1992**, 113.

[7] a) M. Kurihara, S. Daniele, K. Tsuge, H. Sugimoto, K. Tanaka, *Bull. Chem. Soc. Jpn.* **1998**, *71*, 867; b) S. Bhattacharya, *Polyhedron* **1994**, *13*, 451.

[8] a) K. Ray, A. Begum, T. Weyhermüller, S. Piligkos, J. van Slageren, F. Neese, K. Wieghardt, *J. Am. Chem. Soc.* **2005**, *127*, 4403; b) S. Bhattacharya, P. Gupta, F. Basuli, C. G. Pierpont, *Inorg. Chem.* **2002**, *41*, 5810; c) V. Bachler, G. Olbrich, F. Neese, K. Wieghardt, *Inorg. Chem.* **2002**, *41*, 4179; d) J. Tao, H. Maruyama, O. Sato, *J. Am. Chem. Soc.* **2006**, *128*, 1790.

[9] R. Okamura, T. Wada, K. Aikawa, T. Nagata, K. Tanaka, *Inorg. Chem.* **2004**, *43*, 7210.

 © 2007 Wiley-VCH Verlag GmbH & Co. KGaA, Weinheim

[10] S. Maji, B. Sarkar, S. Patra, J. Fiedler, S. M. Mobin, V. G. Puranik, W. Kaim, G. K. Lahiri, *Inorg. Chem.* **2006**, *45*, 1316.
[11] N. Gupta, N. Grover, G. A. Neyhart, P. Singh, H. H. Thorp, *Inorg. Chem.* **1993**, *32*, 310.
[12] a) N. Chanda, S. M. Mobin, V. G. Puranik, A. Dutta, M. Niemeyer, G. K. Lahiri, *Inorg. Chem.* **2004**, *43*, 1056; b) B. Mondal, V. G. Puranik, G. K. Lahiri, *Inorg. Chem.* **2002**, *41*, 5831; c) N. Chanda, B. Mondal, V. G. Puranik, G. K. Lahiri, *Polyhedron* **2002**, *21*, 2033; d) B. Mondal, H. Paul, V. G. Puranik, G. K. Lahiri, *J. Chem. Soc., Dalton Trans.* **2001**, 481; e) B. Mondal, M. G. Walawalkar, G. K. Lahiri, *J. Chem. Soc., Dalton Trans.* **2000**, 4209; f) S. Sarkar, B. Sarkar, N. Chanda, S. Kar, S. M. Mobin, J. Fiedler, W. Kaim, G. K. Lahiri, *Inorg. Chem.* **2005**, *44*, 6092; g) N. Chanda, D. Paul, S. Kar, S. M. Mobin, A. Dutta, V. G. Puranik, K. K. Rao, G. K. Lahiri, *Inorg. Chem.* **2005**, *44*, 3499.
[13] S. Patra, B. Sarkar, S. Ghumaan, M. P. Patil, S. M. Mobin, R. B. Sunoj, W. Kaim, G. K. Lahiri, *Dalton Trans.* **2005**, 1188.
[14] a) C. Sans, M. Rodriguez, I. Romero, A. Llobet, *Inorg. Chem.* **2003**, *42*, 8385; b) C. M. Hartshorn, K. A. Maxwell, P. S. White, J. M. DeSimone, T. J. Meyer, *Inorg. Chem.* **2001**, *40*, 601; c) I. Claustro, G. Abate, E. Sanchez, J. H. Acquaye, *Inorg. Chim. Acta* **2003**, *342*, 29; d) R. Ziessel, V. Grosshenny, M. Hissler, C. Stroh, *Inorg. Chem.* **2004**, *43*, 4262; e) K. Kobayashi, H. Ohtsu, T. Wada, T. Kato, K. Tanaka, *J. Am. Chem. Soc.* **2003**, *125*, 6729; f) C. Bonnefous, A. Chouai, R. P. Thummel, *Inorg. Chem.* **2001**, *40*, 5851; g) J. J. Rack, J. R. Winkler, H. B. Gray, *J. Am. Chem. Soc.* **2001**, *123*, 2432; h) H. Hadadzadeh, M. C. DeRosa, G. P. A. Yap, A. R. Rezvani, R. J. Crutchley, *Inorg. Chem.* **2002**, *41*, 6521; i) A. Gerli, J. Reedijk, M. T. Lakin, A. L. Spek, *Inorg. Chem.* **1995**, *34*, 1836.
[15] S. I. Gorelsky, A. B. P. Lever, M. Ebadi, *Coord. Chem. Rev.* **2002**, *230*, 97.
[16] a) A. B. P. Lever, P. R. Auburn, E. S. Dodsworth, M. Haga, W. Liu, M. Melnik, W. A. Nevin, *J. Am. Chem. Soc.* **1988**, *110*, 8076; b) P. R. Auburn, E. S. Dodsworth, M. Haga, W. Liu, W. A. Nevin, A. B. P. Lever, *Inorg. Chem.* **1991**, *30*, 3502; c) H. Masui, P. R. Auburn, A. B. P. Lever, *Inorg. Chem.* **1991**, *30*, 2402; d) A. B. P. Lever, H. Masui, R. A. Metcalfe, D. J. Stufkens, E. S. Dodsworth, P. R. Auburn, *Coord. Chem. Rev.* **1993**, *125*, 317; e) H. Masui, A. B. P. Lever, E. S. Dodsworth, *Inorg. Chem.* **1993**, *32*, 258.
[17] a) R. Bauernschmitt, R. Ahlrichs, *Chem. Phys. Lett.* **1996**, *256*, 454; b) M. Casida, K. C. Jamorski, K. C. Casida, D. R. Salahub, *J. Chem. Phys.* **1998**, *108*, 4439.
[18] M. B. Robin, P. Day, *Adv. Inorg. Chem. Radiochem.* **1967**, *10*, 247.
[19] S. Ghumaan, B. Sarkar, S. Patra, J. van Slageren, J. Fiedler, W. Kaim, G. K. Lahiri, *Inorg. Chem.* **2005**, *45*, 3210.
[20] S. Chakarborty, R. H. Laye, R. L. Paul, R. G. Gonnade, V. G. Puranik, M. D. Ward, G. K. Lahiri, *J. Chem. Soc., Dalton Trans.* **2002**, 1172.
[21] J. Rusanova, E. Rusanova, S. I. Gorelsky, D. Christendat, R. Popescu, A. A. Rarah, R. Beaulac, C. Reber, A. B. P. Lever, *Inorg. Chem.* **2006**, *45*, 6246.
[22] a) N. Chanda, R. H. Laye, S. Chakraborty, R. L. Paul, J. C. Jeffery, M. D. Ward, G. K. Lahiri, *J. Chem. Soc., Dalton Trans.* **2002**, 3496; b) M. D. Ward, *Inorg. Chem.* **1996**, *35*, 1712; c) N. Chanda, B. Sarkar, J. Fiedler, W. Kaim, G. K. Lahiri, *Dalton Trans.* **2003**, 3550; d) S. Patra, B. Sarkar, S. Maji, J. Fiedler, F. A. Urbanos, R. Jimenez-Aparicio, W. Kaim, G. K. Lahiri, *Chem. Eur. J.* **2006**, *12*, 489.
[23] R. Hariram, B. K. Santra, G. K. Lahiri, *J. Organomet. Chem.* **1997**, *540*, 155.
[24] a) B. Mondal, S. Chakraborty, P. Munshi, M. G. Walawalkar, G. K. Lahiri, *J. Chem. Soc., Dalton Trans.* **2000**, 2327; b) T. B. Hedda, H. L. Bozec, *Inorg. Chim. Acta* **1993**, *204*, 103; c) G. B. Deacon, J. M. Patrick, B. W. Skelton, N. C. Thomas, A. H. White, *Aust. J. Chem.* **1984**, *37*, 929.
[25] a) M.-F. Charlot, Y. Pellegrin, A. Quaranta, W. Leibl, A. Aukauloo, *Chem. Eur. J.* **2006**, *12*, 796; b) P. J. O'Malley, *J. Phys. Chem. B* **2001**, *105*, 11290; c) A. Lozsán, P. Nieto, S. Acevedo, V. Mujica, *J. Phys. Chem. A* **2002**, *106*, 10374.
[26] E. J. P. Malar, *Theor. Chem. Acc.* **2005**, *114*, 213.
[27] a) J. M. Villegas, S. R. Stoyanov, W. Huang, L. L. Lockyear, J. H. Reibenspies, D. P. Rillema, *Inorg. Chem.* **2004**, *43*, 6383; b) S. R. Stoyanov, J. M. Villegas, D. P. Rillema, *Inorg. Chem.* **2002**, *41*, 2941; c) S. R. Stoyanov, J. M. Villegas, D. P. Rillema, *Inorg. Chem. Commun.* **2004**, *7*, 838.
[28] Conversion of the calculated oscillator strength to molar absorptivity was done based on the following references: a) R. S. Drago, *Physical Methods for Chemists*, 2nd ed. Saunders College Publishing, Ft. Worth, **1992**; b) J. E. Monat, J. H. Rodriguez, J. K. McCusker, *J. Phys. Chem. A* **2002**, *106*, 7399.
[29] R. A. Leising, S. A. Kubow, M. R. Churchill, L. A. Buttery, J. W. Ziller, K. J. Takeuchi, *Inorg. Chem.* **1990**, *29*, 1306.
[30] G. M. Sheldrick, SHELX-97, Program for Crystal Structure Solution and Refinement; University of Göttingen, Germany, **1997**.
[31] a) A. D. Becke, *Phys. Rev. A* **1988**, *38*, 3098; b) C. Lee, W. Yang, R. G. Parr, *Phys. Rev. B* **1988**, *37*, 785; c) D. Andrae, U. Haeussermann, M. Dolg, H. Stoll, H. Preuss, *Theor. Chim. Acta* **1990**, *77*, 123; d) P. Fuentealba, H. Preuss, H. Stoll, L. V. Szentpaly, *Chem. Phys. Lett.* **1989**, *89*, 418; e) M. J. Frisch, G. W. Trucks, H. B. Schlegel, G. E. Scuseria, M. A. Robb, J. R. Cheeseman, J. A. Montgomery, Jr., T. Vreven, K. N. Kudin, J. C. Burant, J. M. Millam, S. S. Iyengar, J. Tomasi, V. Barone, B. Mennucci, M. Cossi, G. Scalmani, N. Rega, G. A. Petersson, H. Nakatsuji, M. Hada, M. Ehara, K. Toyota, R. Fukuda, J. Hasegawa, M. Ishida, T. Nakajima, Y. Honda, O. Kitao, H. Nakai, M. Klene, X. Li, J. E. Knox, H. P. Hratchian, J. B. Cross, V. Bakken, C. Adamo, J. Jaramillo, R. Gomperts, R. E. Stratmann, O. Yazyev, A. J. Austin, R. Cammi, C. Pomelli, J. W. Ochterski, P. Y. Ayala, K. Morokuma, G. A. Voth, P. Salvador, J. J. Dannenberg, V. G. Zakrzewski, S. Dapprich, A. D. Daniels, M. C. Strain, O. Farkas, D. K. Malick, A. D. Rabuck, K. Raghavachari, J. B. Foresman, J. V. Ortiz, Q. Cui, A. G. Baboul, S. Clifford, J. Cioslowski, B. B. Stefanov, G. Liu, A. Liashenko, P. Piskorz, I. Komaromi, R. L. Martin, D. J. Fox, T. Keith, M. A. Al-Laham, C. Y. Peng, A. Nanayakkara, M. Challacombe, P. M. W. Gill, B. Johnson, W. Chen, M. W. Wong, C. Gonzalez, J. A. Pople, *Gaussian03* (Revision C.02), Gaussian, Inc., Wallingford, CT, **2004**; f) M. J. Frisch, G. W. Trucks, H. B. Schlegel, G. E. Scuseria, M. A. Robb, J. R. Cheeseman, V. G. Zakrzewski, J. A. Montgomery, Jr., R. E. Stratmann, J. C. Burant, S. Dapprich, J. M. Millam, A. D. Daniels, K. N. Kudin, M. C. Strain, O. Farkas, J. Tomasi, V. Barone, M. Cossi, R. Cammi, B. Mennucci, C. Pomelli, C. Adamo, S. Clifford, J. Ochterski, G. A. Petersson, P. Y. Ayala, Q. Cui, K. Morokuma, P. Salvador, J. J. Dannenberg, D. K. Malick, A. D. Rabuck, K. Raghavachari, J. B. Foresman, J. Cioslowski, J. V. Ortiz, A. G. Baboul, B. B. Stefanov, G. Liu, A. Liashenko, P. Piskorz, I. Komaromi, R. Gomperts, R. L. Martin, D. J. Fox, T. Keith, M. A. Al-Laham, C. Y. Peng, A. Nanayakkara, M. Challacombe, P. M. W. Gill, B. Johnson, W. Chen, M. W. Wong, J. L. Andres, C. Gonzalez, M. Head-Gordon, E. S. Replogle, J. A. Pople, *Gaussian98* (Revision A. 11.4.), Gaussian, Inc., Pittsburgh, PA, **2002**; g) M. Casida, in *Recent Advances in Density Functional Methods* (Ed.: D. P. Chong), World Scientific Press, Singapore, **1995**; vol. I, p. 155; h) G. Schaftenaar, J. H. Noordik, *J. Comput. Aided Mol. Des.* **2000**, *14*, 123; i) S. I. Gorelsky, *AOMIX* program, http://www.sg-chem.net; j) S. I. Gorelsky, A. P. B. Lever, *J. Organomet. Chem.* **2001**, *635*, 187.

Received: September 6, 2006
Published Online: November 17, 2006

 © 2007 Wiley-VCH Verlag GmbH & Co. KGaA, Weinheim